Device Architecture for Improved Redox Couple Mass Transport in Silicon Microwire Photoelectrodes and Electrical Contacts to Silicon Microwire Photovoltaics

Senior Thesis by Andrew C. Meng

California Institute of Technology

Pasadena, California

Submitted May 7, 2013

ACKNOWLEDGEMENTS

First, I would like to thank Professor N.S. Lewis. Nate's insights have been inspiring, and have provided much of the direction of this project. I would like to thank my co-mentors, Dr. C.X. Xiang and Dr. S. Ardo for guidance and advice. Also, I would like to thank members of the group, past and present, for assistance throughout my time at Caltech. Finally, thanks to my family for their support.

This work was supported by the U.S. Department of Energy, Grant DE-FG0203ER15483, by the Caltech Center for Sustainable Energy Research (CCSER), and by Caltech's Summer Undergraduate Research Fellowship program.

PROLOGUE

Applications of silicon microwires to solar energy conversion are investigated in this thesis, which is divided into two chapters. In the first chapter, silicon microwires are investigated as photoelectrodes in photoelectrochemical cells. The mass transport limitations of redox couple is studied in these liquid junction solar cells, and a device architecture proposed and successfully demonstrated to improve device performance. This work was recently published in the Proceedings of the National Academy of Sciences and is reproduced in chapter one (32). In the second chapter, the device architecture developed to improve redox couple mass transport in liquid junction solar cells is explored as a possible method to make electrical contacts to silicon microwire photovoltaics.

TABLE OF CONTENTS

CHAPTER 1

ABSTRACT

Physical integration of a Ag electrical contact internally into a metal/substrate/microstructured Si wire array/oxide/Ag/electrolyte photoelectrochemical solar cell has produced structures that display relatively low ohmic resistance losses, as well as highly efficient mass transport of redox species in the absence of forced convection. Even with front-side illumination, such wire-array based photoelectrochemical solar cells do not require a transparent conducting oxide top contact. In contact with a test electrolyte that contained 50 mM / 5.0 mM of the cobaltocenium$^{+/0}$ redox species in CH_3CN–1.0 M $LiClO_4$, when the counterelectrode was placed in the solution and separated from the photoelectrode, mass transport restrictions of redox species in the internal volume of the Si wire array photoelectrode produced low fill factors, and limited the obtainable current densities to 17.6 mA cm^{-2} even under high illuminations. In contrast, when the physically integrated internal Ag film served as the counter electrode, the redox couple species were regenerated inside the internal volume of the photoelectrode, especially in regions where depletion of the redox species due to mass transport limitations would have otherwise occurred. This behavior allowed the integrated assembly to operate as a two-terminal, stand-alone, photoelectrochemical solar cell. The current density vs voltage behavior of the integrated photoelectrochemical solar cell produced short-circuit current densities in excess of 80 mA cm^{-2} at high light intensities, and resulted in relatively low losses due to concentration overpotentials at 1 Sun illumination. The integrated wire array-based

device architecture also provides design guidance for tandem photoelectrochemical cells for solar-driven water splitting.

INTRODUCTION

To yield optimal solar energy-conversion efficiencies, photoelectrochemical cells require highly effective mass transport of redox species between the photoelectrode and the counter electrode, as well as in the internal void volume of porous, microstructured photoelectrodes. Although the fundamental energy-conversion properties of many semiconductor photoelectrodes are well-documented, the mass transport of reactants and products in highly structured electrochemical systems has received relatively little attention. Diffusion-limited mass transport during the electrochemical deposition of metals onto planar electrodes has been investigated by Scharifker and Hills(1) in the early 1980s, and has been further expanded upon in other studies.(2-5) Penner, et al.(6) have studied the mass-transport properties of conical and hemispherical ultramicroelectrodes in electrochemical cells. Mass transport in nanocrystalline TiO_2-based dye-sensitized solar cells has also been treated theoretically.(7-12) Of specific interest herein is the mass transport of redox species in the internal pore volume of highly microstructured electrodes, such as Si wire array photoelectrodes.

High aspect-ratio semiconductor microwire and nanowire array structures have shown promise in liquid junction devices for solar energy-conversion applications.(13-18) A key attribute of these wire array structures is the orthogonalization of the directions of light absorption and photogenerated charge-carrier collection.(19) However, collection of photogenerated charge carriers will be limited if the solution at the base of the wire arrays, where the path length for the transport of redox couple

species from the bulk solution is largest, is depleted of reactant species during photocurrent flow in the device.

For many types of photoelectrodes, forced convection produced by rapid stirring in a three-electrode configuration,(20) or effective diffusive transport produced by use of a well-designed two-electrode thin-layer cell configuration,(10, 21-23) have been utilized to minimize mass transport losses between the photoelectrode and the counter electrode (Scheme Ia, Ib). However, these approaches do not effectively minimize losses due to restricted mass transport in the internal volume of microstructured photoelectrodes, such as Si wire arrays. As part of this work, we have characterized the mass transport limitations of such systems experimentally as well as with finite-element modeling.

The wire-array photoelectrode architecture also offers an intriguing opportunity to produce integrated, two-electrode, photoelectrochemical solar cell structures that could minimize the ohmic resistance and mass transport losses in the external electrolyte solution. Scheme Ic depicts an architecture that would provide a stand-alone, two-electrode photoelectrochemical solar cell that would require neither external solution volume nor a transparent conductive top contact. In this architecture, the ohmically contacted substrate provides electrical contact to the photoactive wires, and the counter electrode is a deeply physically embedded metal film that contacts the electrolyte in the internal volume of the photoelectrode, but is separated from the substrate, and from the photoactive microwires, by an electrically insulating barrier layer. By minimizing the distance between the working and counter electrodes, and by not requiring any volume of external solution, this device configuration should produce nearly optimal mass

transport of redox species for microstructured photoelectrochemical systems. The ability to generate redox species at the base of the wire array also provides a platform to investigate the mass transport behavior of water-splitting tandem cells in which protons must diffuse from the base of the wire array to reach the photocathode, in order to undergo the reduction reaction needed to complete the fuel production process.

RESULTS

Structure of the Wire Array Electrodes

Figure 1a displays top- and side-view SEM images of the Si microwire arrays that were grown by the VLS process. Figure 1b displays a photograph of a top-down view of a typical Si wire-array substrate, integrated with a Ag film at the base of the wire array. The darker innermost square is the defined photoactive area of Si microwires with interdigitated Ag films; the bordering silver square is the excess Ag film evaporated on the Si substrate; and the outermost striped edge is the Al_2O_3 layer that had been covered by Kapton tape during the Ag evaporation. Figure 1c shows the SEM images of the Ag films, SiO_2 and Al_2O_3 layers at the base of the photoelectrodes. The different layers were identified by the contrast and texture in the image. The Ag/Ti layer had a distinctly textured surface, which is characteristic of polycrystalline metallic films. The two insulating layers had a darker appearance in the cross section, due to charging of the electron beam. The Ag film was electrically insulated from the Si microwire arrays by the SiO_2 and Al_2O_3 layers. The SEM image indicated no physical shorting between the Ag film and the Si microwire arrays. The resistance between the Ag film and the Si microwire arrays was ~10-100 kΩ.

Simulations of Mass Transport in Microwire Array Electrodes

Figure 2a shows the results of COMSOL Multiphysics simulations of the concentration profiles of the oxidized species (cobaltocenium) within the wire-array photoelectrode in the control configuration (Scheme IIa), for which the Si wire-array electrode served as the working electrode, the Pt gauze electrode served as the counter electrode, and the Pt wire served as reference electrode. The bulk concentrations of $CoCp_2^+$ and $CoCp_2^0$ were set to 50 mM and 5.0 mM, respectively. The diffusion coefficients of the $CoCp_2^+$ and $CoCp_2^0$ in CH_3CN were each taken to be 6.4 x 10^{-6} cm^2 s^{-1}. The thickness of the hydrodynamic boundary layer was set to 3.5 μm, which corresponded to the rapid stirring condition used experimentally when the magnetic stir bar was rotating at ~ 3000 rpm close to a planar electrode.

Assuming a uniform current density along the wire-array electrodes and a projected-area current density of 10 mA cm^{-2}, the concentration of $CoCp_2^+$ reached zero at a distance from the tops of the wires equal to ~ 30% of the wire height. In the region of the solution where $[CoCp_2^+] = 0$, the photogenerated charge carriers were forced to recombine, because no oxidized species was present to accept electrons at the wire-array surface. Hence, under these conditions, the photogenerated charge-carrier collection was limited by the mass transport of the redox species in the internal volume of the Si microwire array photoelectrode.

In contrast, Figure 2b shows the simulation results for the concentration profiles of $CoCp_2^+$ within the wire-array photoelectrode in the device configuration (Scheme IIb), for which the Si wire-array electrode served as working electrode, the base Ag film served as counter electrode, and the Pt wire served as the reference electrode. The

minimum in the concentration of $CoCp_2^+$, at a value of $[CoCp_2^+] = 28$ mM, occurred near the mid-point of Si microwire array. Under these operating conditions, the redox species was not fully depleted at any point in the wire-array region.

Figure 2c shows the simulation results for the electric potential profiles of the wire-array photoelectrodes in the stand-alone, two-electrode, solar cell configuration (Scheme Ic). The conductivity of the electrolyte, CH_3CN–1.0 M $LiClO_4$, was set to 5.0 S m^{-1}. Assuming a uniform current density along the wire-array electrode and a projected-area current density of 10 mA cm^{-2}, the maximum electric potential drop, which occurred at the center of the top surface of the wire arrays, due to the solution resistance was less than 2 mV. In contrast, under the same operating conditions, the electric potential drop due the uncompensated resistance in a traditional three-electrode measurement (Scheme IIa) was typically ~ 50 mV even when a Luggin capillary reference electrode was used. Hence, the ohmic resistance loss is significantly reduced due to the integrated wire-array architecture of Scheme Ic. For comparison, operating at a current density of 10 mA cm^{-2}, a 10 μm thick layer of this electrolyte produces a potential drop of ~0.2 mV in a thin-layer configuration between a planar photoelectrode and a planar counterelectrode.

Behavior of Wire Array-Based Photoelectrodes

Figure 3 compares the *J-E* behavior in contact with CH_3CN–1.0 M $LiClO_4$–0.050 M $CoCp_2^+$–0.0050 M $CoCp_2^0$ of the control configuration (black and green traces) with that of the device configuration (blue and red traces), for Si wire-array electrodes that contained Ag films. In the control configuration (Scheme IIa), the Si wire-array electrodes served as the working electrode, the Pt wire served as the reference electrode and the Pt gauze electrode served as the counter electrode. In the device configuration (Scheme IIb), the counter electrode was switched from the Pt gauze electrode to the Ag film, so that the redox species were regenerated at the base of the photoelectrode. In the absence of stirring, the *J-E* characteristics of photoelectrodes in the control configuration exhibited large hysteresis, due to the limited mass transport within the microwire arrays. Thus, the mass transport limitations of the redox species significantly lowered the photoelectrochemical performance of the photoelectrodes. In contrast, the *J-E* characteristics of photoelectrodes in the device configuration exhibited nearly no hysteresis, and showed much larger short-circuit current densities and fill factors.

Table 1 summarizes the open-circuit photovoltage, V_{OC}, short-circuit photocurrent density, J_{SC}, and the fill factor, *ff*, values for the two different photoelectrode configurations (Scheme IIa and Scheme IIb) under different illumination and stirring conditions. In the absence of forced convection by stirring, at a light intensity equivalent to 4 Suns, the photoelectrodes produced J_{sc} values that were 2.5 times higher in the device configuration (Scheme IIb) than in the control configuration (Scheme IIa). In the presence of rapid stirring, when the magnetic stir bar was rotating close to the

photoelectrode at ~ 3000 rpm, at 1 Sun the two photoelectrode configurations produced mutually similar *J-E* behavior. In contrast, at 4 Suns, a relatively small but significant improvement in the *J-E* behavior was observed for device configuration relative to the control configuration.

Behavior of Wire Array-Based Photoelectrochemical Solar Cells

Figure 4 shows the effect of illumination intensity on the current density vs voltage (*J-V*) characteristics of Si wire-array photoelectrodes with internal Ag films, when operated in a stand-alone, two-electrode, solar cell configuration (Scheme Ic). In the stand-alone two-electrode configuration, a droplet of propylene carbonate (PC)–1.0 M $LiClO_4$–0.150 M $CoCp_2^+$–0.150 M $CoCp_2^0$ was used to make the semiconductor/liquid junctions. The maximum illumination intensity from the W-halogen ELH-type illumination corresponded to 900 mW cm^{-2}, i.e. 9 Sun, with the light intensity attenuated to lower values, such as 100 mW cm^{-2}, using neutral density filters. Propylene carbonate was used as the solvent because its low volatility minimized evaporation of the liquid in the electrochemical device. Under illumination, the short-circuit current density scaled linearly as a function of the light intensity, reaching 89.1 mA cm^{-2} at 9 Sun, with no significant loss due to mass transport (Figure 4, insert). In the absence of solution, no appreciable shorting current was observed between the Si microwire arrays and the Ag film (Figure 4, dashed trace).

DISCUSSION

Si Wire-Array Based Solar Cells

The architecture of structured microwire arrays offers a unique opportunity to achieve deep physical integration of the light absorber, the electrolyte, and the electrical contacts in a photoelectrochemical system that optimizes mass transport of redox species and that minimizes losses due to solution resistance, while obviating the need for a transparent conducting material as the top contact in the solar cell device. The device structure easily sustained short-circuit current densities of ~ 50 mA cm^{-2} at 50 mM concentrations of redox species in the solution (Figure 3). For comparison, a thin-layer cell with an electrolyte spacing of 10 μm and a redox species having a concentration of 50 mM and a diffusion coefficient of 6.4 x 10^{-6} cm^2 s^{-1} would provide a mass transport limited current density of ~ 30 mA cm^{-2}, whereas a disk electrode rotating at 3000 rpm would provide a mass-transport-limited current density of ~ 45 mA cm^{-2} at the same concentration of redox-active species in solution, assuming a kinematic viscosity value of 4.5 x 10^{-3} cm^2 s^{-1} for CH_3CN. In practice, it is desirable to have the mass-transport-limited current densities be significantly larger than the short-circuit photocurrent densities, to minimize mass-transport overpotentials that would decrease the fill factor, and thus the energy-conversion efficiencies, of the photoelectrode when used as a stand-alone, two terminal, photoelectrochemical solar cell.(20, 21, 24)

The short-circuit photocurrent density of the wire-array photoelectrode was ~ 10 mA cm^{-2} in the stand-alone, two-electrode configuration under 1 Sun illumination. The observed J_{sc} can be further improved by light trapping techniques.(25-28) Using an

antireflective coating, a Ag back-reflector and embedded light-scatterers, these wire-array substrates have exhibited up to 96% peak absorption and have been shown to absorb up to 85% of day-integrated, above-bandgap direct-beam sunlight.(25) Moreover, the long minority-carrier diffusion length and the low surface recombination velocity of the vapor-liquid-solid (VLS) grown Si microwires has produced broadband, near-unity internal quantum yields for carrier collection through a radial semiconductor/liquid junction.(13, 25, 28) The embedded Ag counter electrode in Scheme Ic inherently serves as an effective back-reflector, thereby improving the light absorption in the Si wire-array photoelectrodes. By utilization of an additional antireflective coating and light-scatterers, the energy-conversion efficiency of the Si wire-array photoelectrodes in the stand-alone, two-terminal configuration is expected to be improved significantly. The physical integration of the Ag film in Scheme Ic also provides a blueprint for a "wrap-around contact" for a solid-state Si microwire photovoltaic, in which instead of a transparent conducting oxide top contact, the Ag metal layer at the base of the microwire arrays would contact the emitter region of the microwires, thereby providing the "top" contacts to the device.

Mass Transport Effects in Wire Array Photoelectrodes

Most photoelectrochemical cells are designed to allow evaluation of the performance of the semiconductor photoelectrode while minimizing effects that might arise from the electrolyte, such as the series resistance, concentration overpotentials, optical absorption, etc.(20, 29) In contrast, high aspect-ratio Si wire-array photoelectrodes present challenges for mass transport of redox species. Hence, the Ag film counter electrodes that were incorporated at the base of the Si wire-array photoelectrodes reduced the effective diffusive path length of redox species to a value equal to half of the wire-array length, in the case of uniform photogeneration of charge carriers along the length of the wires. Kelzenberg, et al.(25, 30) have calculated the photogeneration profiles of 25 μm long Si microwire arrays using 3D finite-difference time-domain (FDTD) methods. The photogeneration profiles in such systems depend significantly on the incident angle of the illumination source.(25) The concentration gradient of redox species in the internal volume of the microwire arrays, and the resulting change in optical absorption along the wire length, further complicate the absorption properties of the Si microwire electrodes. Although a quantitative analysis of light absorption coupled with mass transport is outside the scope of this study, the significant improvement of the short-circuit current densities and fill factors in the absence of stirring, and/or under high illumination intensities (Figure 3), demonstrated the effectiveness of the fabricated device configuration. Still further improvement of the *J-E* behavior could be realized by further reductions in the effective ion path length, such as by the use of a p-n^+ wire-array electrode, in which photogenerated carriers could travel vertically in the emitter layer along large segments of the wire length.

The increase in the short-circuit current densities for the device configuration relative to the control configuration (Figure 3) is attributable to the improved mass transport of the redox species, as well as to a reduction at steady-state, in the optical absorption of the redox system in the device configuration. As shown in Table 1, under ELH-simulated 1 Sun illumination and with effective stirring, the short-circuit current densities of the Si wire-array photoelectrodes were nearly identical in the control configuration and the device configuration, indicating negligible reduction of optical absorption of the solution species at the base of the electrode in device configuration at low illumination intensities. Under ELH-simulated 4 Sun illumination and rapid stirring, the Si wire-array photoelectrodes in the device configuration exhibited a J_{sc} value of 48.7 mA cm^{-2}, which was greater than four times the J_{sc} value under 1 Sun illumination, 10.4 mA cm^{-2}. The extra gain of the current density, 7.1 mA cm^{-2} relative to four times the J_{sc} value under 1 Sun, is attributable to reduction of the optical absorption of the solution species, due to the active regeneration in the device configuration of $CoCp_2^+$, which is less absorptive in the visible region than $CoCp_2^0$. The stand-alone two-electrode results exhibited a similar increase in short-circuit current densities relative to the control configuration. The slope of a plot of J_{sc} vs illumination light intensity (Table 1) increased with increasing light intensity, consistent with expectations for the enhanced depletion of the more absorptive species, $CoCp_2^0$, at the base of the microwire arrays in the device and stand-alone solar cell configurations, relative to the control configuration.

The concentration profiles of $CoCp_2^+$ (Figure 2) suggest that, due to mass transport limitations, the short-circuit current densities should be significantly reduced in

the control configuration because the pores in between the wires were calculated to be depleted of solution species over a distance corresponding to ~70% of the length of the wires. However, experiments showed that under 1 Sun illumination and under rapid stirring, the short-circuit current densities in the control configuration were comparable to those of the device configuration (Table 1). This discrepancy between the simulations and the observations can likely be attributed to a non-uniform current density distribution along the length of the microwire array, as well as to the long minority-carrier diffusion length of the p-Si microwire arrays. A long minority-carrier diffusion length (> 30 μm), as has been observed in similar p-Si microwire arrays,(31) will allow lateral mobility of the photogenerated charge carriers along the wire length, and thus will relax the mass transport limitations relative to those indicated by simulations, which assumed a constant flux of photogenerated charge carriers along the length of the wires in the array.

In conclusion, the physical integration of metal contacts into ordered microporous photoelectrodes provides an interesting opportunity to achieve optimized mass transport of reactants and products, as well as to minimize the ohmic potential drops due to the solution resistance in the cell. The metal contacts embedded at the base of the photoelectrodes also inherently served as an effective back-reflector that enhanced the optical absorption of the Si microwire array devices. In contact with a test electrolyte, PC–1.0 M $LiClO_4$–0.150 M $CoCp_2^+$–0.150 M $CoCp_2^0$, the integrated microwire photoelectrodes exhibited nearly ideal short-circuit current density in a stand-alone, two-terminal photoelectrochemical solar cell without any carrier collection loss due to the redox couple mass transport. The highly integrated microwire arrays, electrolyte, and

embedded electrical contact system thus provides a promising device architecture for photosynthetic systems, such as solar-driven water-splitting photoelectrochemical cells.

EXPERIMENTAL

Computational Modeling of Mass Transport in Wire-Array Structures

The 3-D diffusion equations of the wire-array geometries of interest were solved using the COMSOL Multiphysics finite-element-analysis software package, in conjunction with MATLAB. Three types of boundary conditions were applied in the numerical simulation. Symmetric boundary conditions were imposed for the four sidewalls of the simulation region. Dirichlet (or first-type) boundary conditions were employed at the hydrodynamic boundary layer, where the concentrations of the reduced and oxidized species, respectively, were equal to their concentrations in the bulk of the solution. For the Dirichlet boundary condition, beyond the hydrodynamic boundary layer thickness, Δ_0, (determined experimentally), convection was assumed to maintain uniform concentrations of both redox species at values that were equal to their bulk concentrations (also determined experimentally). Neumann (or second-type) boundary conditions were employed for the redox couple flux at the photoelectrode surface. For the Neumann boundary condition, a uniform current flux was assumed at the wire-array surface. For wire-array electrodes that had metal films at the bases of the wires, the Neumann boundary condition and the continuity equation were imposed at the base of the electrode, so that the inward cathodic flux was equal to the outward anodic flux. Other constants, including the geometries of the wires, as well as the diffusion coefficients and concentrations of the redox species, were set to the experimentally determined values.

The ohmic resistance loss in Scheme Ic was simulated by solving the 3-D Poisson's equation in COMSOL Multiphysics. A periodic boundary condition was

employed for the four sidewalls of the simulation region. The top of the simulation regions was assumed to be a perfect electrical insulator. Electrical ground was established at the metal counter electrode. The Neumann boundary condition for the uniform current flux was applied at the Si microwire electrode surface, where the current density at the electrode surface was normalized by the geometry factors such that the current density per unit of projected area was equal to 10 mA cm^{-2}. The conductivity of the electrolyte was set to a value of 5.0 S m^{-1} in the subdomain settings.

Preparation of p-Si Wire-Array Photoelectrodes

To obtain patterned wire growth, p^+-Si (111) wafers with a resistivity of < 0.001 Ω cm were coated with 300 nm of thermal oxide. A layer of S1813 photoresist (Rohm and Haas) was then deposited onto the oxide, and the photoresist was exposed through a chromium photolithography mask, followed by an oxide dry etch, to produce an array of 3 μm diameter holes on a 7 μm pitch square lattice. Buffered HF (Transene) was used to remove unmasked oxide, before thermal evaporation of 350 nm of Cu (6N, Kurt Lesker) and subsequent lift-off.

The growth substrates were then cleaved into ~ 2 cm x 2 cm chips that were rinsed with acetone and isopropyl alcohol, and then introduced into a vapor-liquid-solid (VLS) chemical vapor deposition (CVD) growth chamber. The base pressure of the CVD chamber was <10 mTorr. The substrates were then annealed for 20 min in H_2 (g) (500 sccm) at 1000 °C. Wire growth was performed at atmospheric pressure at 1000 °C by introduction of a 500 sccm H_2 (g) carrier gas flow and a 50 sccm $SiCl_4$ (g) precursor gas flow. The dopant density of the wires was controlled by varying the flow rate of the in situ dopant, BCl_3. The length of the wires was controlled by varying the duration of the growth.

Following growth, the substrates were cooled slowly under H_2 (g) to 750 °C, to allow the Cu VLS catalyst to diffuse out of the wires. The wires were then cooled under He to room temperature. The Cu VLS catalyst tips were removed by etching the samples for 30 min in 1.5 M $FeCl_3$ (aq), followed by etching for 10 s in 5.8 M HF (aq). The outer surface of the wire was etched in 8 M KOH (aq) for 1 min at room

temperature. The Si wire arrays were then fabricated into electrodes as described previously.(13-15)

Formation and Characterization of Ag Metal Films in the Internal Volume of p-Si Wire-Array Photoelectrodes

To produce films of Ag that were physically embedded into the internal volume of the Si microwire arrays, chips of p-Si wire arrays that were not mounted as electrodes were cleaved into ~ 1 cm x 1 cm squares. The wire-array samples were then thermally oxidized at 1100 °C under O_2 (4000 sccm) for 90 min, followed by electron-beam evaporation of > 500 nm Al_2O_3 (99.99%, Kurt Lesker) over the entire sample. After masking off the edges of the device substrate with Kapton tape, a 5 nm Ti (99.99%, Kurt Lesker) adhesion layer, followed by a 200 nm film of Ag (99.99%, Kurt Lesker), was deposited by electron-beam evaporation.

The modified Si wire-array electrodes were etched in 2 M HNO_3(aq) for 3 s, to remove residue Ag from the sidewalls of the Si microwires. The substrate area that had been previously masked off by Kapton tape was then covered with epoxy (Hysol 9460F, McMaster-Carr). Ohmic contact was made by scratching the back side of the substrate with Ga:In eutectic. Cu/Sn wire was then attached with conductive Ag paste to make an external back contact to the electrodes. Contact to the interdigited Ag film that was located between the Si microwires, as well as to the side of the oxide-isolated substrate was made by affixing a Cu/Sn wire to the Ag by use of silver solder (McMaster-Carr). Both Cu/Sn wires were fed through the back of a supporting glass tube, and were sealed with epoxy (Hysol 9460F, McMaster-Carr) to prevent electrical shorting.

Scanning electron microscope (SEM) images were collected using a field-emission SEM (Hitachi S-4100). Optical microscopy images were collected using an Olympus BX-51 microscope.

Photoelectrochemistry.

For all nonaqueous photoelectrochemical experiments, CH_3CN (anhydrous, 99.8%, Sigma Aldrich) was distilled under N_2 (g) (ultra-high purity, Air Liquide) from CaH_2 (≥97%, Fluka). Battery-grade $LiClO_4$ (anhydrous, 99.99%) was purchased from Sigma Aldrich, and was used as received. Battery-grade electrolyte solution (1.0 M $LiClO_4$ premixed in propylene carbonate, PC) was purchased from Novolyte Technologies, and was used as received. Bis(cyclopentadienyl) cobalt(II) (cobaltocene, $CoCp_2^0$) was purchased from Sigma Aldrich and was purified by sublimation. Bis(cyclopentadienyl) cobalt(III) hexafluorophosphate (cobaltocenium, $CoCp_2^+ \cdot PF_6^-$) was purchased from Sigma Aldrich and was recrystallized before use.

Current density vs. potential (*J-E*) data were collected at a scan rate of 40 mV s^{-1} using a Gamry (Reference 600) potentiostat. In addition to the working electrode, the electrochemical cell contained a stir bar, a Pt gauze electrode, and a Pt wire electrode that was allowed to equilibrate with the solution potential of the $CoCp_2^{+/0}$ redox couple. The stir bar was positioned adjacent to the photoelectrode and was rotated at ~ 3000 rpm to facilitate mass-transport of the redox couple. The rotation of the stir bar was controlled with an external bar magnet that had been to an electric motor (NWSL 12270-9) driven by a DC power supply (Rail Power 1370). The electrochemical cell was contained inside a VAC Omni-Lab glovebox that had < 0.5 ppm of O_2 (g). Air mass (AM) 1.5 equivalent illumination was provided from a Sylvania ELH-type W-halogen lamp with a quartz diffuser. The light intensity was monitored by a Si photodiode that was placed at the same position in the electrochemical cell as the working electrode.

Two cell configurations, the control figuration and the device configuration, were evaluated to compare the energy-conversion performance of the Si wire-array electrodes. In the control configuration (Scheme IIa), the Si wire-array electrode served as the working electrode, the Pt gauze electrode served as the counter electrode, and the Pt wire served as reference electrode. In the device configuration (Scheme IIb), the Si wire-array electrode served as the working electrode, the base Ag film served as the counter electrode, and the Pt wire served as the reference electrode.

J-E data were also evaluated in a stand-alone two-electrode configuration in which the Si wire-array electrode served as the photocathode and the bottom Ag film served as the counter electrode (Scheme Ic). In this configuration, a calibrated Si photodiode was placed next to the Si wire array electrode, and a droplet of solution that contained the $CoCp_2^{+/0}$ redox couple was used to make liquid contact to the electrodes.

The photoactive area (~ 0.5 cm x 0.5 cm) of wire-array substrates was prepared by scratching the wires off of the substrate with a ceramic-coated stainless steel razor blade. The area was determined by scanning the photoelectrodes with a commercially available scanner (Epson V300). A clear definition of the photoactive part of the wire array also served to prevent electrical shorting through the sides of the substrate.

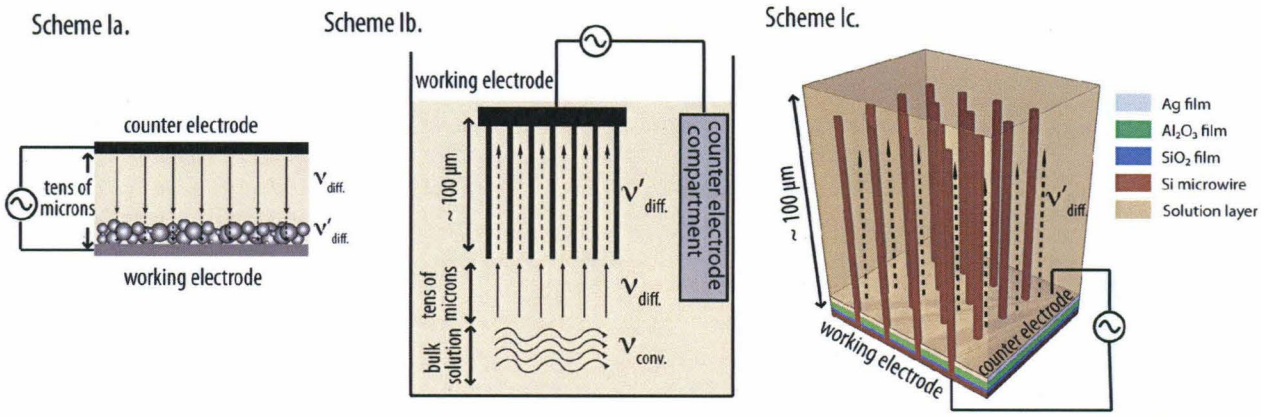

Scheme I. Schematics of three electrochemical systems that facilitate mass transport between the photoelectrodes and the counter electrodes, where $\upsilon_{conv.}$ illustrates convective mass transport by rapid stirring, $\upsilon_{diff.}$ illustrates diffusive mass transport in solution and $\upsilon'_{diff.}$ illustrates diffusive mass transport within microporous photoelectrodes. Scheme Ia depicts a two-electrode thin-layer configuration that exploits effective diffusive transport. Scheme Ib shows a conventional three-electrode configuration that uses rapid convective stirring. Scheme Ic illustrates a stand-alone, two-terminal photoelectrochemical solar cell configuration that uses a deeply embedded Ag film as the counter electrode. The typical direction of illumination was normal to the working electrode.

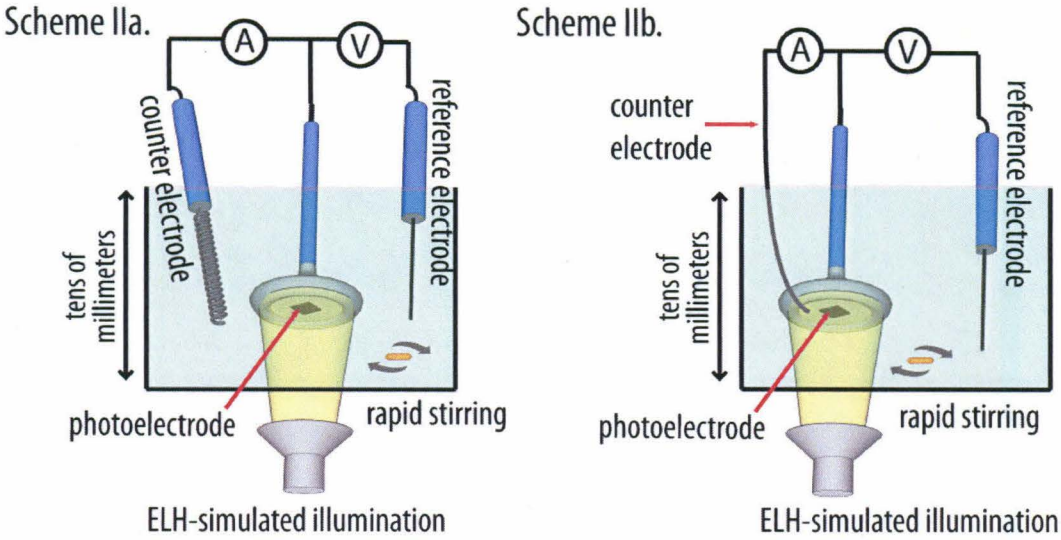

Scheme II. Schematics of the two photoelectrochemical configurations evaluated in this work. Scheme IIa illustrates the control configuration, for which the Si wire-array electrode served as the working electrode, the Pt gauze electrode served as the counter electrode and the Pt wire served as reference electrode. Scheme IIb illustrates the device configuration, for which the Si wire-array electrode served as the working electrode, the Ag film served as the counter electrode and the Pt wire served as reference electrode. Both configurations employed a W-halogen ELH-type illumination source.

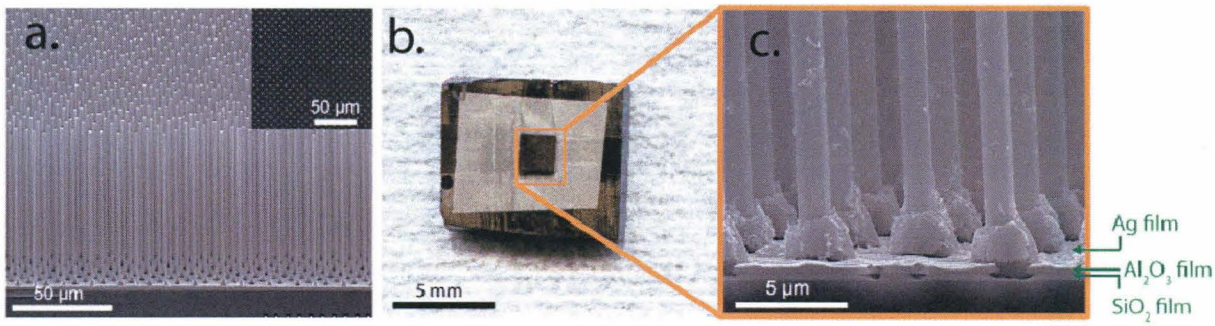

FIG. 1. (a) Scanning electron microscope image showing the Si microwire arrays that were grown by VLS process. (b) Optical microscopy image showing a typical Si wire-array substrate embedded with a silver film that had been electrically isolated from the wire-array electrode. (c) Scanning electron microscope image showing the silver film at the base the electrode, with the Ag electrically insulated from the Si microwire arrays by the Al_2O_3 and SiO_2 isolation layers.

.

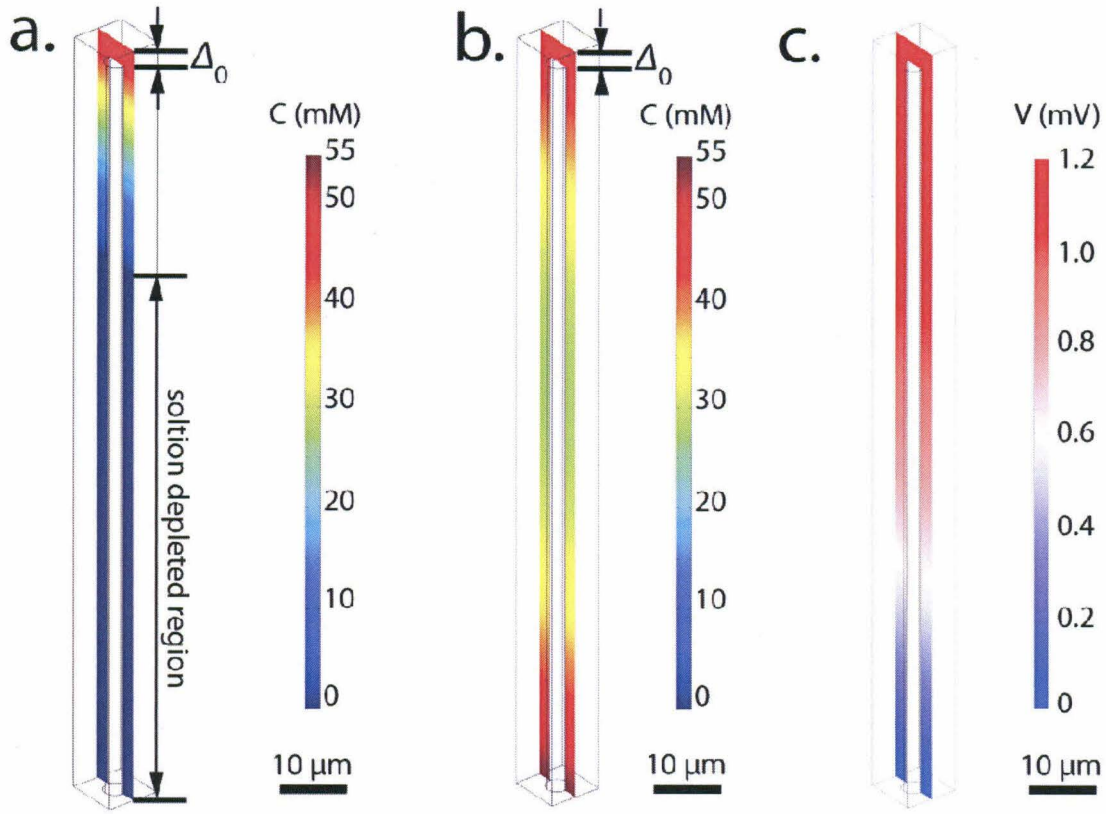

FIG. 2. Finite element simulation (in COMSOL Multiphysics) of the concentration profiles of oxidized species in operating Si microwire photoelectrodes (a) in the control configuration and (b) in the device configuration, where Δ_0 denotes the hydrodynamic boundary layer thickness. (c) Simulation of the electric potential profiles of the wire-array photoelectrodes in the stand-alone, two-electrode configuration (Scheme Ic).

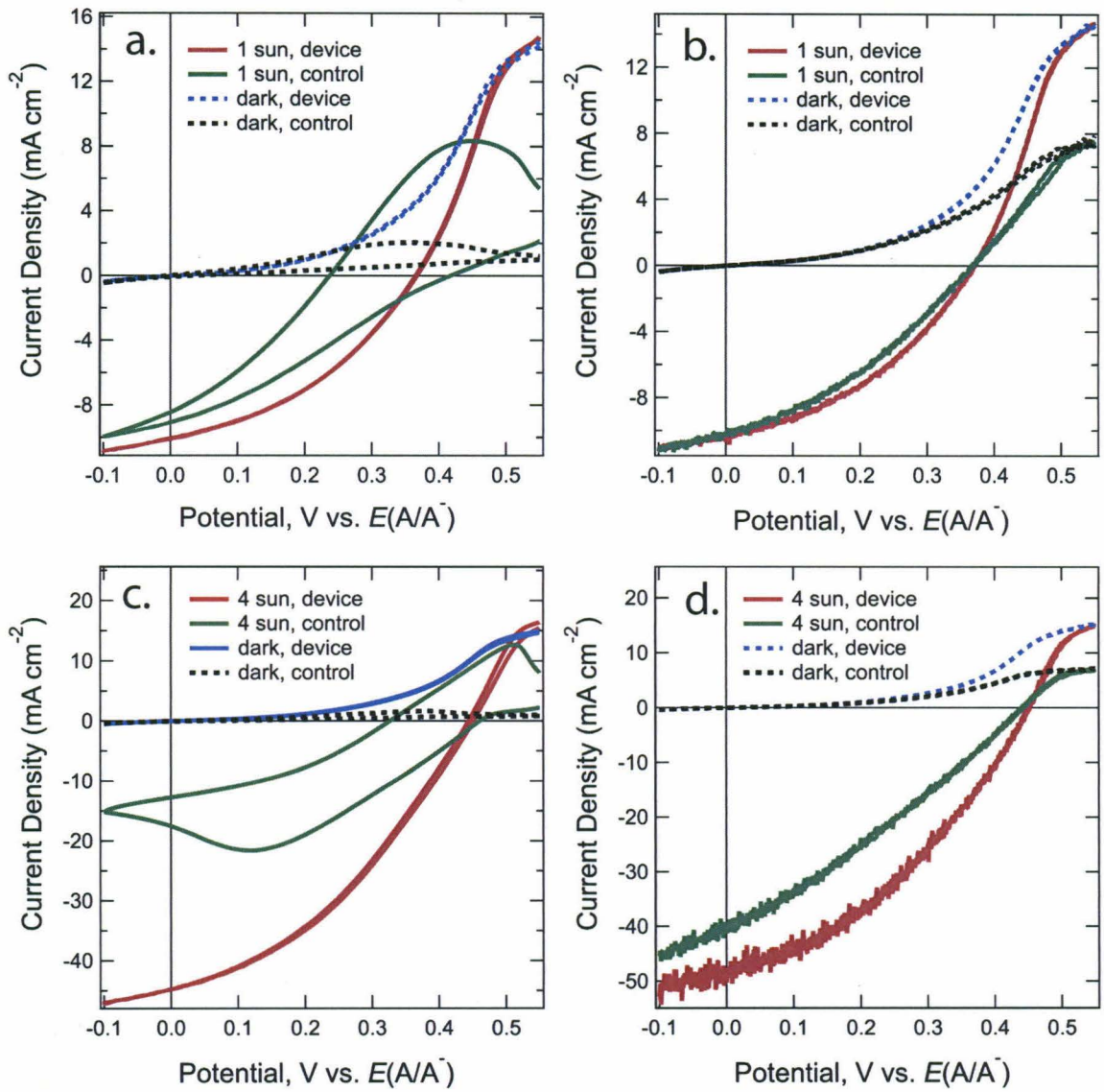

FIG. 3. Current density–potential characteristics of Si wire-array photoelectrodes in the control configuration and in the device configuration. Photoelectrodes were in contact with CH_3CN–1.0 M $LiClO_4$–0.050 M $CoCp_2^+$–0.0050 M $CoCp_2^0$, a) under ELH-simulated 1 sun illumination and without stirring, b) under ELH-simulated 1 sun illumination and with rapid stirring, c) under ELH-simulated 4 sun illumination and without stirring, d) under ELH-simulated 1 sun illumination and with rapid stirring.

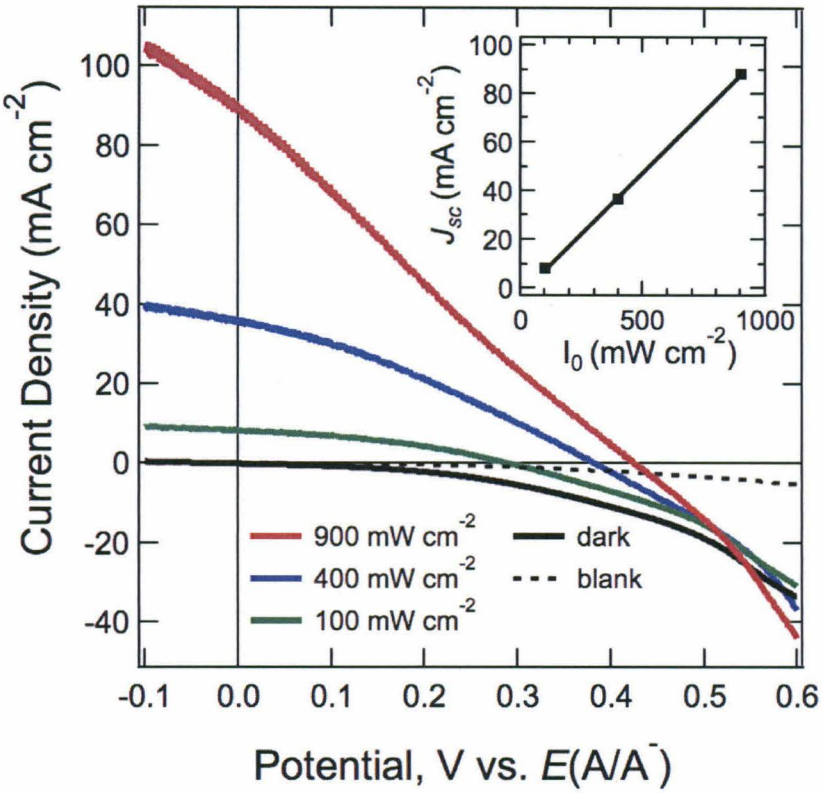

FIG. 4. Illumination intensity dependence of the current density–potential characteristics of Si wire-array photoelectrodes that contained integrated Ag films as a counter electrode, in a stand-alone two-electrode configuration in contact with the propylene carbonate–1.0 M $LiClO_4$–0.150 M $CoCp_2^+$–0.150 M $CoCp_2^0$ electrolyte. The insert

Table 1. Open-circuit voltage, V_{oc}, short-circuit photocurrent density, J_{sc} and fill factor, *ff* data for Si wire-array photoelectrodes in the control configuration and in the device configuration.

		V_{OC} (V)			J_{SC} (mA cm^{-2})			*ff*		
Illumination Intensity		1 Sun	2 Sun	4 Sun	1 Sun	2 Sun	4 Sun	1 Sun	2 Sun	4 Sun
Device	No stirring	0.37	0.41	0.45	10.1	20.9	44.7	0.39	0.38	0.38
	Rapid stirring	0.37	0.41	0.45	10.4	22.0	48.7	0.38	0.39	0.37
Control	No stirring**	0.42	0.44	0.46	9.1	16.6	17.6	0.28	0.30	n/a
	Rapid stirring	0.37	0.41	0.44	10.2	20.7	40.6	0.35	0.33	0.29

** For the *J-E* behaviors with significant hysteresis, the forward scan results were used to obtain V_{oc}, J_{sc} and *ff* data.

CHAPTER 2

ABSTRACT

Integrated metal films as ohmic contacts to core shell radial pn junction Si microwire array photovoltaics hold potential for cost-effective, large-area devices. The highest efficiency Si microwire photovoltaics to-date use a transparent conducting oxide top contact, which involves intensive processing. Furthermore, indium tin oxide contacts cannot be used in a flexible polymer embedded device due to mechanical fracturing when the device is peeled from the substrate. It has been demonstrated that a thin metal film can be integrated into a Si microwire array without electrical shorting. Evaporated Al_2O_3 films were employed to electrically insulate the substrate base. Then, Ag films were deposited as wrap-around contacts to only the emitter layer of core shell radial pn junction silicon microwires. These Ag films also served as a back reflectors redirecting light to the solar cells. Wrap-around contact devices exhibited open circuit voltage of 220 mV and short circuit current density of 0.6 mA cm^{-2} under 400 mW cm^{-2} of ELH simulated solar illumination. The lower than expected energy conversion efficiency can be attributed to Ag film blocking light absorption. Enhanced light absorption in wrap-around contact devices are expected increase the short circuit current density compared to conventional pn junction Si microwire devices, leading to higher device efficiencies.

INTRODUCTION

In recent years, solar energy has been a major focus of sustainable energy research. As a solar absorber material, Si microwire arrays have the advantage of decoupling light absorption and charge carrier collection (13-15). Si microwire solar cells also require less Si, and can be fabricated cheaply using chemical vapor deposition (CVD). We investigate the process of electrically contacting core-shell p-n^+ Si microwires in a solid-state device configuration. Electron beam evaporation of Ag is used to make contact to the n^+ emitter shell of the microwire. Eutectic GaIn is used to contact the back of the Si wire array substrate, and energy conversion properties can be characterized.

In the highest efficiency cells to-date, electrical contact to Si microwires can be made by embedding the wire array in a polymer, etching the polymer back to expose the microwire tips, and sputtering a transparent conducting oxide as a top-contact (28). Alternatively, an electron beam evaporated Al_2O_3 electrical insulation layer that blocks electrically shorting pathways from the n+ emitter shell to the p-type core of the microwire will allow an evaporated metal film to contact the n+ emitter shell only (Scheme III). There are several advantages of the proposed bottom-contact over the top-contact. The top-contact is process intensive and requires a highly transparent and conductive material, which may be limited in abundance.

RESULTS

Prior to Ag film integration, pn junction devices were tested electrochemically in 100 mM / 0.4 mM dimethylferrocene ($Me_2Fc^{+/0}$) redox couple in methanol to verify the solar energy conversion properties and to check for macroscopic electrical shorting. Open circuit voltage of 340 mV and short circuit current density of 4.4 mA cm^{-2} were observed (Figure 5a). Since the emitter layer is not optimized, the solar energy conversion efficiency of the device is lower than expected. However, the devices are sufficient for further processing for wrap-around contact devices. The champion wrap-around contact device yielded an open circuit voltage of 220 mV and short circuit current density of 0.6 mA cm^{-2} at 4 Suns light intensity (Figure 5b). The open circuit voltage and short circuit current density of the pn junction is significantly decreased after the wrap-around contact processing. This can be attributed to parasitic light absorption from a conformal film of Ag coating the sidewalls of the Si microwires, reducing light absorption (Figure 6).

DISCUSSION

It is expected that the wrap-around contact device architecture will lead to an increase in short-circuit current density due to increased light absorption from the Ag film serving as a back-reflector. This is not observed, the efficiency is much lower than expected. This can be attributed to the Ag film covering parts of the photoactive Si, and preventing light from being absorbed in the Si and rendering the back-reflector effect insignificant. A thick, conformal layer of Ag on the sidewalls of the Si microwires is observed by scanning electron microscopy. In order to prevent the deleterious effects of the Ag film, a dilute HNO3 etch is expected to remove Ag from the tips and sidewalls of the Si microwires without removing the Ag film embedded as the wrap-around contact.

EXPERIMENTAL

Wire growth was executed first by patterning a n^+ Si 300nm thermal oxide substrate with S1813 photoresist using a 3 μm dot square array Cr mask. Evaporation of high purity Cu (6N) catalyst onto patterned substrate was followed by lift-off in preparation for Si vapor-liquid-solid (VLS) growth by chemical vapor deposition (CVD). The chamber was pumped down to base pressures of roughly 0.5 mTorr with growth at atmospheric pressure and 1000°C. The chamber was first pressurized with H_2 (carrier gas); 50 sccm $SiCl_4$ (precursor); 2 sccm BCl_3 (in situ dopant). Cool down consisted of slow cooling for 20 minutes to 750°C under H_2 to allow Cu VLS catalyst to diffuse out of the wires and then fast cooling to room temperature under He.

Prior to dry oxide growth for pn junction wire array processing, wire-array substrates were scratched off on the edges to allow electrical contact to be made to the Ag film wrap-around contact later. Oxide diffusion barrier incorporated wires were synthesized by oxidizing complete wire substrates, and then infilling with 5 mL toluene, 1 g PDMS polymer, 0.1 g Sylgard 184 curing angent. Subsequent etch steps first removed oxide not protected by PDMS with HF (10%) for 5 min., and then PDMS with PDMS etchant (1:1 tetrabutylammonium fluoride (TBAF) in tetrahydrofuran (THF)/dimethylformamide (DMF), v/v) for 30 min. Radial pn junctions were fabricated by heating in a furnace at 1000°C while flowing 20 sccm BCl_3 and 400 sccm H_2 for 30 minutes to diffuse B into the oxide diffusion barrier incorporated wires to create a p^+ emitter layer.

Wrap-around contact solar cells were fabricated by processing radial pn junction Si microwires. A protective electrical insulation layer of 1 μm Al_2O_3 was deposited to

prevent shorting from the Ag film to the base or to the p-Si microwire core. A 2 s etch in 10% HF removed any Al_2O_3 from the sidewalls of the microwires to allow electrical contact to the n^+ emitter layer. A 250 nm Ag film was then deposited as a wrap-around contact to the radial pn junction Si microwire array.

CONCLUSION

Wrap-around contact silicon microwire photovoltaics offer a promising route to inexpensive solar energy through highly scalable large-area devices. Open circuit voltages of wrap-around contact silicon microwire devices are observed in the range of 200 mV at 4 Sun illumination intensity, which is much lower than expected. Short circuit current density is in the range of 1 mA cm^{-2}, also lower than expected. These results are promising since they are consistent with scanning electron microscope images suggesting parasitic light absorption from the evaporated Ag film contacts. The processing for such devices is much less process intensive compared to the current state-of-the-art, and higher efficiencies are expected from the device architecture. Furthermore, the wrap-around contact can be applied to silicon microwires with coated with an amorphous silicon p-i-n structure for tandem cell photovoltaics or a photoelectrosynthetic device.

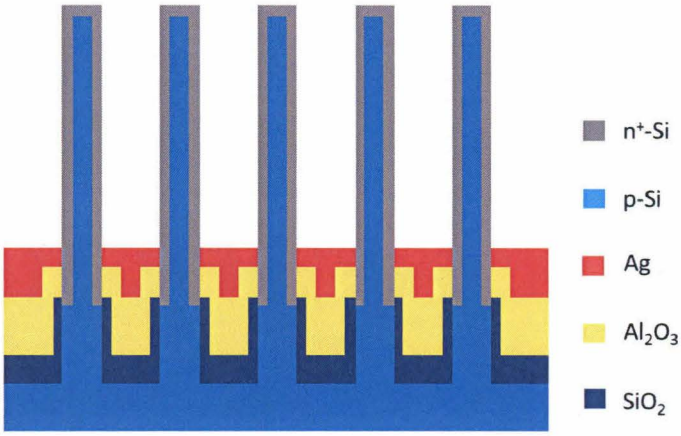

Scheme III. The wrap-around contact for radial junction Si microwire solar cells. Al_2O_3 insulates the base substrate and prevents it from electrically shorting to the Ag film.

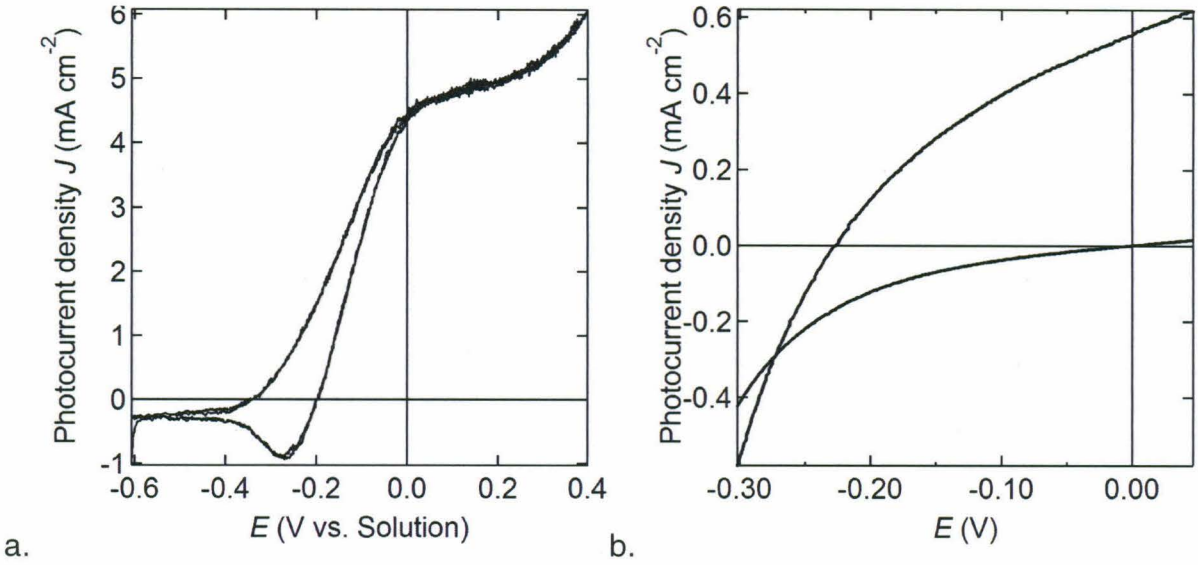

FIG 5. (a) Current density-potential characteristics of pn junction silicon microwire devices in 100 mM / 0.4 mM dimethylferrocene ($Me_2Fc^{+/0}$) redox couple under 100 mW cm^{-2} of W-halogen ELH-type simulated solar illumination. (b) Current density-potential characteristics of pn junction silicon microwire solid state devices under 400 mW cm^{-2} of ELH simulated solar illumination and in the absence of illumination.

a. 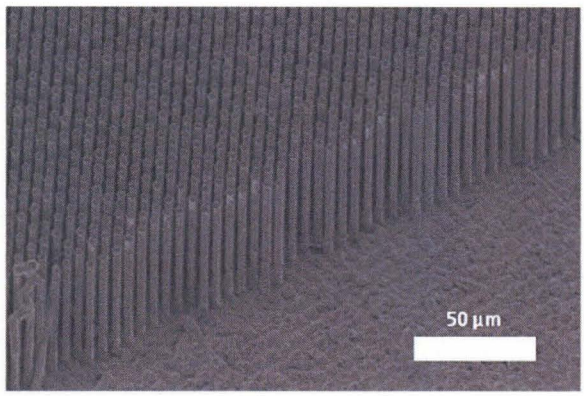

b. 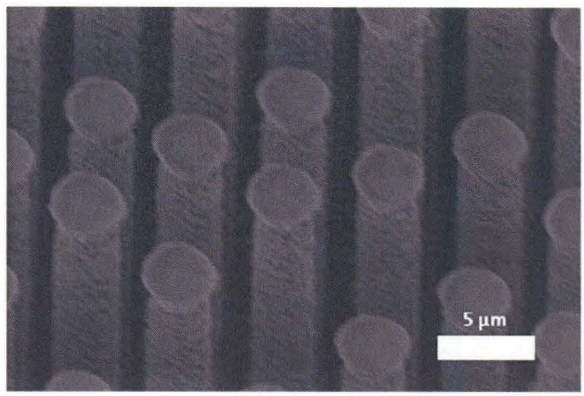

FIG 6. (a) Scanning electron microscope image of final wrap-around contact device structure. (b) Inset of (a). From the images, the evaporated Ag texture conformally coats the length of the sidewalls of the Si microwires.

REFERENCES

1. Scharifker BR & Hills GJ (1981) Electrochemical kinetics at microscopically small electrodes. *J. Electroanal. Chem.* 130:81-97.

2. Heerman L & Tarallo A (1999) Theory of the chronoamperometric transient for electrochemical nucleation with diffusion-controlled growth. *J. Electroanal. Chem.* 470(1):70-76.

3. Scharifker BR & Mostany J (1984) 3-Dimensional Nucleation with Diffusion Controlled Growth .1. Number Density of Active-Sites and Nucleation Rates Per Site. *J. Electroanal. Chem.* 177(1-2):13-23.

4. Heerman L & Tarallo A (2000) Electrochemical nucleation with diffusion-limited growth. Properties and analysis of transients. *Electrochem. Commun.* 2(2):85-89.

5. Sluytersrehbach M, Wijenberg JHOJ, Bosco E, & Sluyters JH (1987) The Theory of Chronoamperometry for the Investigation of Electrocrystallization - Mathematical-Description and Analysis in the Case of Diffusion-Controlled Growth. *J. Electroanal. Chem.* 236(1-2):1-20.

6. Penner RM, Heben MJ, & Lewis NS (1989) Preparation and Electrochemical Characterization of Conical and Hemispherical Ultramicroelectrodes. *Anal. Chem.* 61(15):1630-1636.

7. Kalaignan GP & Kang YS (2006) A review on mass transport in dye-sensitized nanocrystalline solar cells. *J. Photochem. Photobiol. C Photochem. Rev.* 7(1):17-22.

8. Lin Y, *et al.* (2006) Computer simulations of light scattering and mass transport of dye-sensitized nanocrystalline solar cells. *J. Electroanal. Chem.* 588(1):51-58.

9. Hyk W & Augustynski J (2006) Steady-state operation of porous photoelectrochemical cells under the conditions of mixed diffusional and migrational mass transport - Theory. *J. Electrochem. Soc.* 153(12):A2326-A2341.

10. Papageorgiou N, Gratzel M, & Infelta PP (1996) On the relevance of mass transport in thin layer nanocrystalline photoelectrochemical solar cells. *Sol. Energy Mater. Sol. Cells* 44(4):405-438.

11. Lee JJ, Coia GM, & Lewis NS (2004) Current density versus potential characteristics of dye-sensitized nanostructured semiconductor photoelectrodes. 1. Analytical expressions. *J. Phys. Chem. B* 108(17):5269-5281.

12. Lee JJ, Coia GM, & Lewis NS (2004) Current density versus potential characteristics of dye-sensitized nanostructured semiconductor photoelectrodes. 2. Simulations. *J. Phys. Chem. B* 108(17):5282-5293.

13. Boettcher SW, *et al.* (2010) Energy-Conversion Properties of Vapor-Liquid-Solid-Grown Silicon Wire-Array Photocathodes. *Science* 327(5962):185-187.

14. Maiolo JR, Atwater HA, & Lewis NS (2008) Macroporous silicon as a model for silicon wire array solar cells. *J. Phys. Chem. C* 112(15):6194-6201.

15. Maiolo JR, *et al.* (2007) High aspect ratio silicon wire array photoelectrochemical cells. *J. Am. Chem. Soc.* 129(41):12346-12353.

16. Garnett E & Yang PD (2010) Light Trapping in Silicon Nanowire Solar Cells. *Nano Lett.* 10(3):1082-1087.

17. Yuhas BD & Yang PD (2009) Nanowire-Based All-Oxide Solar Cells. *J. Am. Chem. Soc.* 131(10):3756-3761.

18. Garnett EC & Yang PD (2008) Silicon nanowire radial p-n junction solar cells. *J. Am. Chem. Soc.* 130(29):9224-9227.

19. Kayes BM, Atwater HA, & Lewis NS (2005) Comparison of the device physics principles of planar and radial p-n junction nanorod solar cells. *J. Appl. Phys.* 97(11):114302.

20. Bard AJ & Faulkner LR (2000) *Electrochemical Methods, Fundamentals and Applications* (Wiley) 2nd edition Ed.

21. Gibbons JF, Cogan GW, Gronet CM, & Lewis NS (1984) A 14-Percent Efficient Nonaqueous Semiconductor Liquid Junction Solar-Cell. *Appl. Phys. Lett.* 45(10):1095-1097.

22. Gratzel M (2001) Photoelectrochemical cells. *Nature* 414(6861):338-344.

23. Parkinson B (1982) An Evaluation of Various Configurations for Photo-Electrochemical Photo-Voltaic Solar-Cells. *Sol Cells* 6(2):177-189.

24. Fajardo AM & Lewis NS (1997) Free-energy dependence of electron-transfer rate constants at Si/liquid interfaces. *J. Phys. Chem. B* 101(51):11136-11151.

25. Kelzenberg MD, *et al.* (2010) Enhanced absorption and carrier collection in Si wire arrays for photovoltaic applications. *Nat Mater* 9(3):239-244.

26. Boettcher SW, *et al.* (2011) Photoelectrochemical Hydrogen Evolution Using Si Microwire Arrays. *J. Am. Chem. Soc.* 133(5):1216-1219.

27. Kelzenberg MD, *et al.* (2011) High-performance Si microwire photovoltaics. *Energ Environ Sci* 4(3):866-871.

28. Putnam MC, *et al.* (2010) Si microwire-array solar cells. *Energ Environ Sci* 3(8):1037-1041.

29. Tan MX, *et al.* (1994) Principles and Applications of Semiconductor Photoelectrochemistry. *Prog Inorg Chem* 41:21-144.

30. Kelzenberg MD, Putnam MC, Turner-Evans DB, Lewis NS, & Atwater HA (2009) Predicted efficiency of Si wire array solar cells. *Proceedings of the 34th IEEE PVSC.*

31. Atwater H (2011) Si microwire-array solar cells. *Abstr Pap Am Chem S* 241.

32. Xiang CX, Meng AC, & Lewis NS (2012) Evaluation and optimization of mass transport of redox species in silicon microwire-array photoelectrodes. *Proc Natl Acad Sci USA.* 109: 15622-15627.